CHARACTERIZING THE DYNAMIC PROPERTIES OF TORON-UMBILIC PAIRS

Timothy Boyle

A thesis submitted to the

Faculty of the Honors Program of the

University of Colorado in partial fulfillment

of the requirement for the degree of

Bachelor of Arts, Physics Department of Physics and

Liquid Crystal Materials Research Center

Defense Date: 3/8/2016

Thesis Advisor: Ivan Smalyukh
Committee Members: Paul Beale (Physics) , Daniel Jones (Music, Honors), Ivan Smalyukh (Physics)

Abstract

Topological defects are studied in many different fields of physics and have recently attracted the attention of researchers due to the interesting applications they provide[15]. Liquid crystals, classified as a mesophase, provide a model experimental system for discovering the physics governing these defects. The research presented in this thesis characterizes the dynamic properties of defect ensembles dubbed “toron-umbilic pairs” and unveils the mechanisms behind their motion. Two different manifestations of motion were observed and are described by their relationships to the systems’ parameters and by the interactions exhibited by the defects themselves.

Acknowledgements

I would like to thank professor Smalyukh for providing me with the opportunity to work on this project and for guiding me in my experimental endeavors. I would also like to thank Paul Ackerman, who cooperated with me on this project and provided me with help every step of the way. In addition, I would like to thank everyone in the Smalyukh research group for their assistance with the lab equipment and for granting me time to conduct my research in the lab.

Contents

1. Introduction

1.1 Liquid Crystals

A liquid crystal (LC) is a phase of matter between that of a solid and a liquid. This material phase can be achieved by heating particular crystalline materials past their melting point but not beyond the threshold for the liquid to become isotropic. Alternatively, the LC phase can be achieved through inorganic solutions of amphiphilic molecules[6]. While the nomenclature of liquid crystals may seem absurd, it is quite accurate in that the materials possess qualities of both liquids and crystals. LCs exhibit fluidity and the inability to support shear akin to liquids yet maintain properties of crystals such as anisotropy in optical properties and periodic arrangement of molecules in one spatial direction[7].

Many different phases can exist within the liquid crystals phase itself. The nematic phase is described as having long-range orientation order amongst constituent molecules (see Figure 1a)[10]. To describe the LC, the average molecular orientation is assigned to a unit vector with head-tail symmetry. These directionless vectors constitute the systems' director, which can spatially vary and can contain topological defects. Cholesteric or chiral-nematic liquid crystals have the tendency to have helically twisted director fields. In other words, it is energetically preferably for adjacent molecules to align at a slight angle. The distance over which the molecules twist 2π radians is dubbed the "pitch" (see Figure 1b)[10].

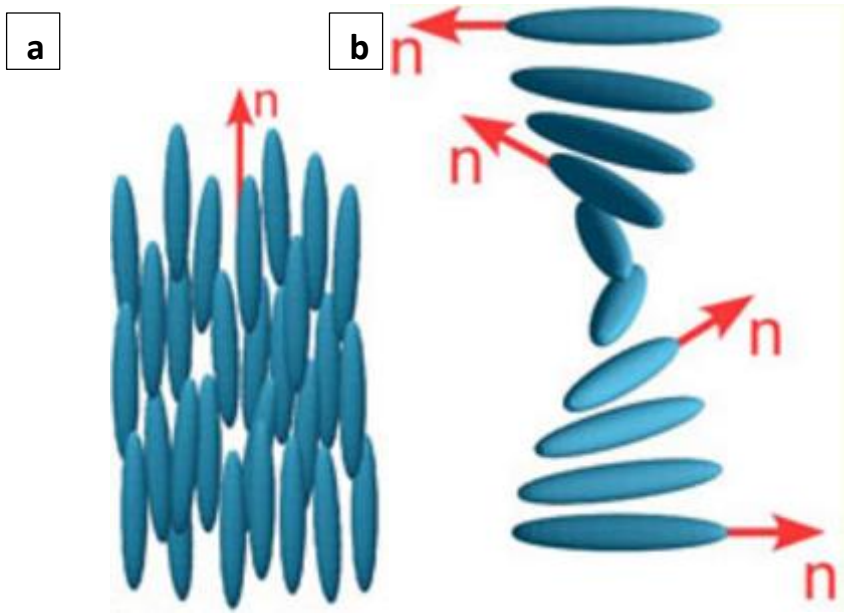

Figure 1 | (**a**) The nematic liquid crystal phase. The molecules are all oriented in a single direction, however the molecules themselves have no positional order. Each molecule points vertically resulting in a director along the n-axis. (**b**) The cholesteric liquid crystal phase. The molecules exhibit twist along the vertical axis. The distance shown in this diagram is half of the material's pitch.

Many other properties are assigned to liquid crystals, including dielectric anisotropy, viscosity, and magnetic susceptibility[6]. Of great importance to this project is the dielectric anisotropy (Δε). The sign (positive or negative) of a liquid crystal's dielectric anisotropy determines the direction in which the molecules align themselves relative to the direction of an applied electric field. An LC with a – Δε will align its molecules perpendicular to the direction of an applied field, while a material with a +Δε exhibits parallel alignment.

1.2 Topology

A singular topological defect is a discontinuity or "tear" in the director field[11]. Nonsingular defects can occur through "escape" into the third dimension[16]. Defects are generally spontaneously formed when the director field is strongly distorted due to a symmetry breaking transition from a disordered state[15]. As their name suggests, defects are generally

undesirable as they reduce optical quality and may interfere with the system of study. However, topological defects have attracted attention as they provide interesting applications, such as the fast response of a cholesteric blue phase being utilized in liquid crystal displays (LCDs)[15]. Associated with defects is a topological "charge", which describes the particular disturbance in the director field. +1 point defects can be imagined as a sphere with strong homeotropic or planar boundary conditions, causing the director to be singular at a point. In the presence of a +1 defect, a -1 defect spawns, as topological defect charge is conserved in a uniform far field (see Figure 2)[15].

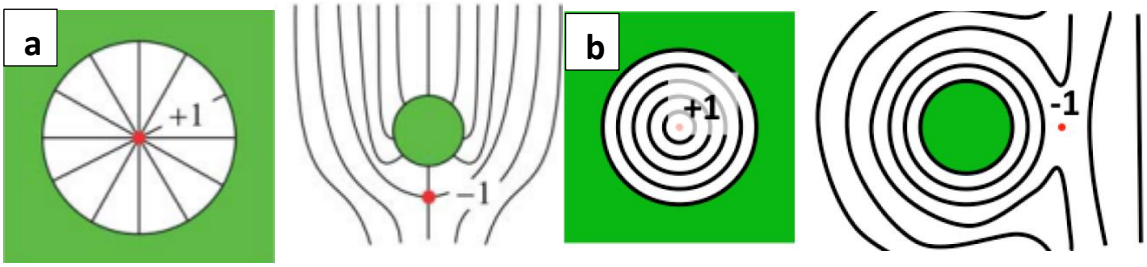

Figure 2 (**a**) A point defect of charge +1 manifesting as a result of homeotropic surface boundary conditions. Within a uniform far field, this defect creates a -1 point defect. Images taken from [15]. (**b**) A point defect of charge +1 as a result of planar surface boundary conditions, which also creates a -1 point defect.

Many unique and interesting topological structures can be formed within liquid crystals. For instance, a Skyrmion is recognized as a topological structure having a director field that twists π radians from its center (see Figure 3a)[8]. Similarly, double-twist cylinders exhibit 2-D twist in the directions perpendicular to the cylindrical axis (see Figure 3)[9]. Recently, the manifestation of a self-assembled topological particle dubbed a "toron" was studied in great detail. Using a high-resolution imaging apparatus, researchers were able to unveil many details of its topological structure[1].

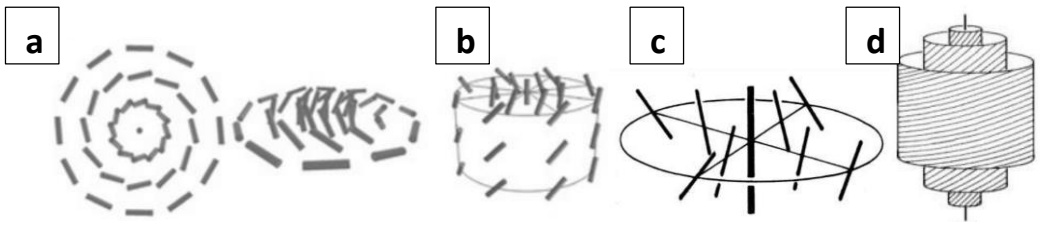

Figure 3 | Images taken from [9]. (**a**) A half-Skyrmion excitation illustrated from two different viewing directions. The cylinders describe the director *n*. (**b**) A double-twist cylinder. The director field twists in all directions perpendicular to the vertical axis of the double-twist cylinder[8]. (**c**) Double-twist. The molecules are twisted with respect to one another in two dimensions, compared to one dimensional twist in the helical phase. (**d**) Double twist-tube[9].

1.3 Toron-Umbilic Pairs

It was discovered that torons consist of double-twist cylinders looped on themselves (see Figure 4). By means of local energetic excitation, a confined cholesteric can self-assemble into a toroidal structure (see Figure 4b)[1]. The director field twists 180^{o} from the center to the outside of the toron. At the center, the director field is vertically aligned, perpendicular to the plane of the cylindrical axis. As a result of this configuration, two point defects manifest along the vertical axis of the toron and help to embed this configuration in the surrounding, vertically-aligned liquid crystal (see Figure 4c,d).

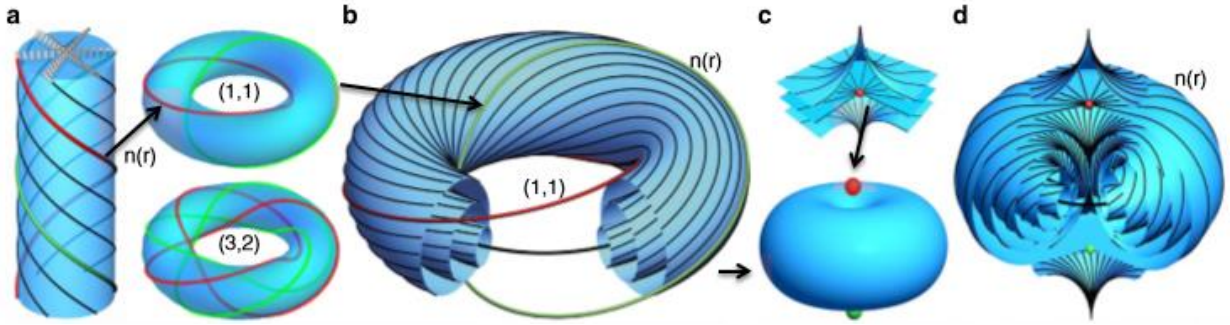

Figure 4 | Images taken from [1]. (**a**) A double-twist cylinder. (**b**) A double-twist torus (toron) formed by a double-twist cylinder looped on itself. (**c**) Defects of charge +/- 1 that are above and below the torus in uniform homeotropic far field that enable the loop of double twist to meet the vertical surface boundary conditions. (**d**) The director field structure of the toron.[1]

For the experiments of this thesis, a liquid crystal with a negative dielectric anisotropy was confined between two glass substrates coated with polyimide to provide strong homeotropic anchoring (see Figure 5e). In isolation, the liquid crystal director points vertically or perpendicular to the plane of the substrates due to the strong homeotropic anchoring. Upon the application of a vertical 1 kHz electric field, and since $\Delta\varepsilon$ is negative, the liquid crystal director tilts in the mid-plane of the cell to minimize free energy. The molecules in the bulk align themselves perpendicularly to the applied field, while the molecules tangent to the substrates maintain their vertical alignment due to the homeotropic surface anchoring. Along with in-plane tilt, the director also twists as a result of the nature of cholesteric materials; they prefer adjacent molecules to be at slight angles with one another. It is normal for topological defects to spontaneously occur during this transition as a result of broken symmetry and the random mid-plane tilt directionality.

When a toron is present in the sample and an electric field is applied, the surrounding system responds by tilting and twisting its molecules to align the director field in the direction perpendicular to that of the electric field (see Figure 5g). During this process, random defects spawn within the sample as a result of broken symmetry, as seen in Figure 5b. As time progresses, the defects annihilate with one another, however, one of the defects approaches the toron until the two rest adjacently. The region surrounding the toron umbilic pair is referred to as a translationally invariant cholesteric (TIC) due to the twisted orientation of the molecules present throughout the entire region and the translationally uniform mid-plane tilt directionality (see Figure 5d).

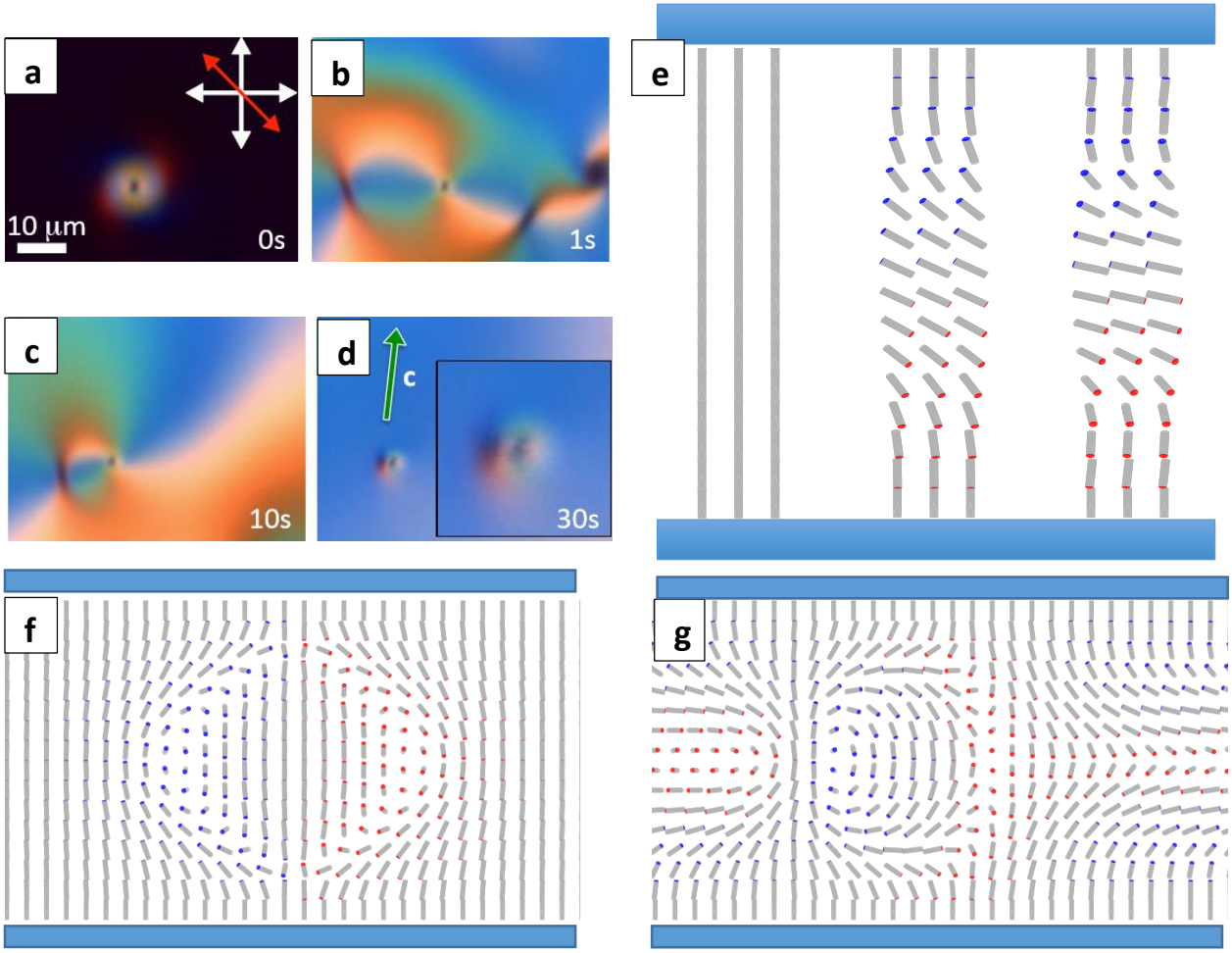

Figure 5 | (**a**) A toron, viewed between crossed polarizers with a waveplate. The double-headed white arrows denote the transmission axis of polarizers and the wave plate slow axis is denoted by the red double headed arrow. (**b**) 1 kHz square wave signal at 4 V_{rms} amplitude applied to the same region of the cell for one second. In plane tilt and twist surrounds the toron and forms non-singular umbilic defects in the resulting c-field due to the broken symmetry. (**c**) After 10 seconds of applied voltage, two of the umbilics have annihilated. (**d**) After 30 seconds the toron and remaining umbilic have come together to form a defect dipole embedded in a TIC with mid-plane tilt oriented along the green arrow. The inset shows an enlarged view of this defect dipole. (**e**) A cross section of a liquid crystal cell confined between two glass substrates with homeotropic anchoring responding to the presence of a vertically aligned AC electric field. The red and blue cylinder caps are used to guide the readers eyes and represent the director pointing into and out of the page. (**f**) The director field of a toron within a cholesteric liquid crystal confined between glass substrates with strong homeotropic surface anchoring – no applied electric field. (**g**) The same system as (f) in the presence of a 1 kHz electric field.

The magnitude of the applied voltage affects the size of both the toron and the umbilic as shown in Figure 6d. The radius of the toron and overall size of the umbilic decreased as a

function of amplitude. Notice that the umbilic covered about the same fraction of the toron's perimeter, but since perimeter decreased, the width of the umbilic also decreased. Above 4.2 V, the toron and umbilic annihilated.

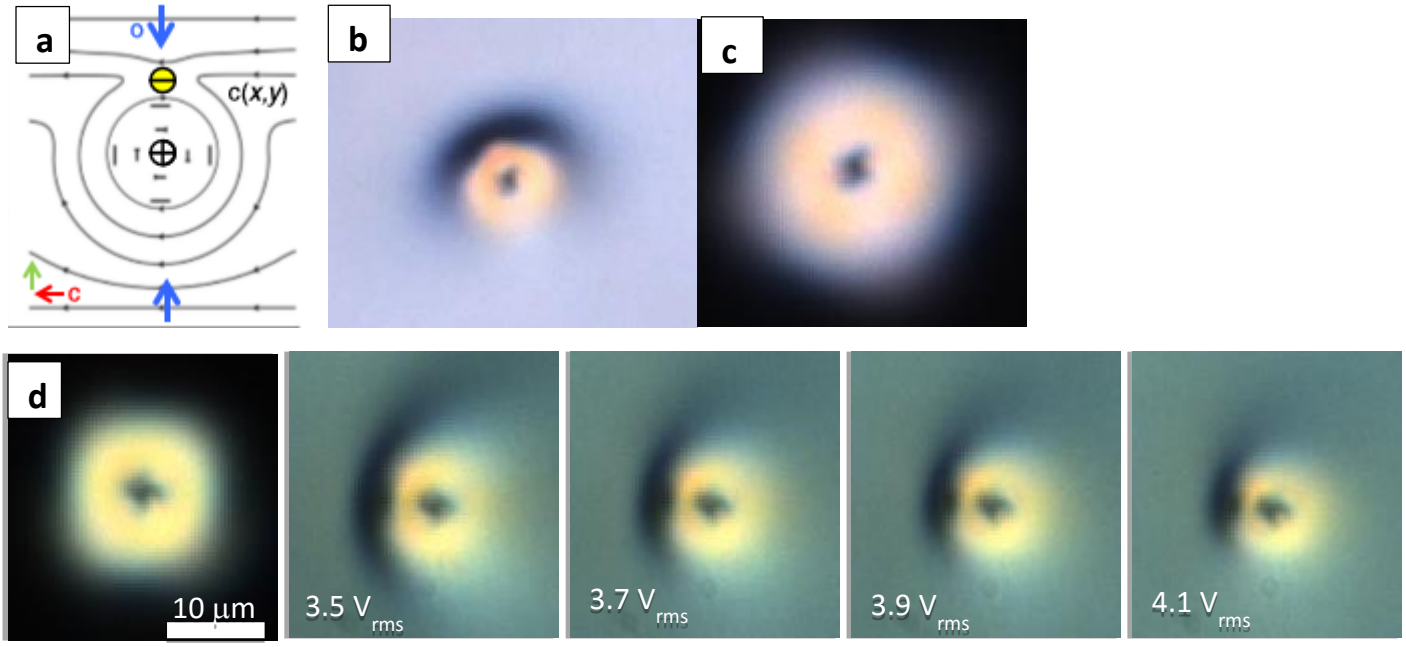

Figure 6 | (**a**) A torn embedded in a TIC. The director field circularly encompasses the toron, yet has to realign with the far c-field, resulting in a discontinuity at a point around the toron. The far c-field points perpendicularly to the dimension connecting the centers of the toron and umbilic. (**b**) A toron-umbilic pair embedded in a TIC viewed under cross polarizers.[1] (**c**) A toron viewed under crossed polarizers with no applied electric field. (**d**) Images of a toron-umbilic pair in equilibrium for different applied voltages.

1.4 Toron-Umbilic Dynamics

The application of a gated electric field resulted in the oscillation between states of a toron-umbilic pair embedded in TIC and an isolated toron surrounded by a vertical director field. As the field was turned off, the toron and its umbilic began to separate; the TIC began to vanish and the umbilic delocalized (see Figure 6c). Upon reapplying the electric field, the umbilic appeared within the vicinity of the toron. The pair then began drifting toward one another until returning to equilibrium (see Figure 6b). After this process was complete, a net

displacement was observed. The cycle then repeated, with the field turning off once again. Over time, the toron-umbilic pair was able to traverse through the liquid crystal medium (see Figure 7a). The motion resembled that of an inch-worm or a swimmer performing the breaststroke, and here forth will be referred to as a "swimming" motion.

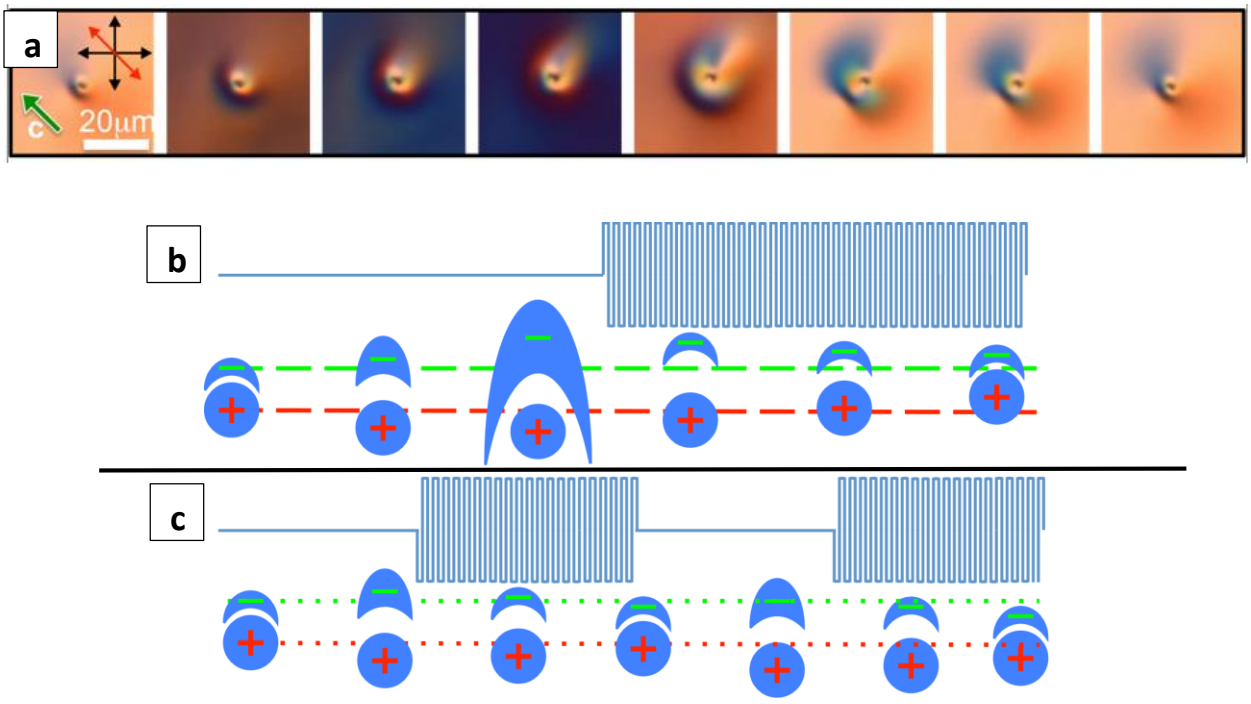

Figure 7 | (**a**) Images of a toron-umbilic pair performing one swimming-cycle. The double-headed black arrows denote the transmission axis of polarizers, the red double-headed arrow denotes the wave plate slow axis and the green arrow indicates the orientation of the c-field. (**b**) A model of the prediction of the mechanism behind swimming motion. The signal above begins in the off-state and the toron and its umbilic (represented by the red + and green – respectively) begin to separate. When the electric field turns on, the toron quickly travels towards the umbilic, leaving the system displaced from its initial position. (**c**) A model of the prediction of the mechanism behind the motion observed for high gate-frequency values. As the toron and umbilic initially separate, the toron is quickly repelled while the umiblic exhibits less mobility. When the pair returns to equilibrium, the system is displaced in the direction of the toron due to the toron's initial repulsion.

An initial model of this motion was developed and is diagramed in Figure 7b. It was theorized that as the toron and umbilic separate with no applied field, the umbilic moves further away from its initial position. Upon reinstating the electric field, it was hypothesized

that the toron moves more quickly towards the umbilic. Thus, the pairs' displacement occurs in the direction of the umbilic. This theory suggests the existence of a speed anisotropy (difference in speed) of the toron and umbilic defects.

In addition to the swimming motion exhibited by toron-umbilic pairs, it was observed that the defects drift in the direction of the toron for high gate frequency values. When the on and off-times are short as a result of a high gate frequency, the toron and umbilic do not have sufficient time to separate. Instead, they tend to vibrate and slowly travel in the direction opposite that of swimming motion. A theoretical model is provided in Figure 7c.

1.5 Thesis Overview

The research for this thesis investigates the dynamic properties of toron-umbilic pairs. The following sections will discuss the procedures and results of the experiments and compare the results to related research in order to better understand the system. This report will also provide applications and ideas for future work to continue the project.

2. Methods

2.1 Sample Preparation and Apparatus

The liquid crystal used for the experiments consisted of a nematic host with a negative dielectric anisotropy (AMLC-0010, from Alpha Micron Industries) mixed with the chiral additive ZLI-811, resulting in a cholesteric liquid crystal with a pitch of 10 μm. The cell, or microscope slide, was constructed using two glass substrates coated with indium tin oxide (ITO). ITO is both electrically conductive and optically transparent, allowing for the application of electric

fields between the substrates without inhibiting the transmission of light. The ITO surfaces were treated with polyimide SE-1211 to provide strong homeotropic anchoring of the director field. SE1211 was spin-coated at 2,700 rpm for 30 seconds and then pre-baked at 90 °C for 5 minutes. Following the pre-bake, the substrates were baked for 1 hour at 180 °C. The width of the cell was set at 10 μm by glass fiber segments dispersed in ultraviolet-curable glue. The cell was then filled with approximately 2 micro-liters of LC by means of capillary forces and then sealed with epoxy. Two wire leads were soldered onto the inner surfaces of the substrates using an ultra-sonic soldering iron to allow for the application of potential differences across the cell via a function generator.

The microscope used was an inverted Olympus microscope equipped with a "dry" (non-immersion oil) 50x objective in order to supply a detailed view of the sample while still allowing for motion to be observed over long distances. Crossed polarizers were arranged in the microscope to improve the clarity of the picture of the toron. Video was recorded using a mounted charge-coupled device (CCD) which captured about 90x90 μm^2 of the sample. A home-made LabView-based function generator and data acquisition board (NIDAQ-6363, National Instruments) were used for the creation and application of different voltage waveforms via the wires soldered onto the sample. An optical tweezer apparatus was used to both generate and trap torons, with trapping providing the ability to reposition torons within the cell. The tweezers consisted of a 1064 nm holographic fiber-laser and were able to "trap" particles due to a localized electromagnetic-intensity gradient[9]. The power output was controlled via a homemade LabView program and was kept below 50 mW to avoid melting of the LC and surface pinning of defects.

2.2 Experiments

2.2.1 Parameter Sweep

The goal of the parameter-sweep experiments was to determine how the motion of toron-umbilic pairs depended on the parameters of the gated electric-field signal and to uncover details of the motion of the particles. The parameters studied were the amplitude, V_{rms}, gate frequency, f_g, duty cycle, dc, and off-time, t_{off} (see Figure 8). The amplitude is represented by V_{rms}, the root-mean-square voltage of the signal. The duty cycle is the ratio of the on-time and the total period, with the total period being one $1/f_g$. Gate frequency and duty cycle, however, can be coupled to represent the on and off-times (t_{on} and t_{off}), as shown by the following equations: $t_{on} = dc*T$ and $t_{off} = (1-dc)*T$. A square waveform was chosen for the carrier signal to avoid intermediate values possessed by other waveforms such as sine and triangle waves.

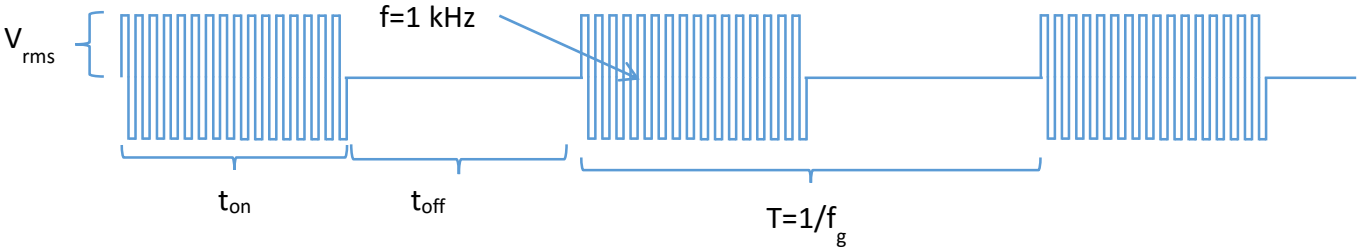

Figure 8 | The gated high-frequency electric field signal consisting of a superposition of two signals: a 1 kHz square-wave and a binary signal with frequency f_g.

To begin the parameter-sweep experiments, a toron had to be generated. This was achieved with the optical tweezers, capable of perturbing a small region of the LC causing the director field to self-assemble into a closed-loop og double-twist cylinder as a way of minimizing free-energy[1]. With a toron present in the sample, a constant 1 kHz electric field

with V_{rms} = 4 V was applied, resulting in a TIC. The transition from a non-TIC to a TIC spawned a variable number of topological defects, known as umbilics, which would annihilate each other if given ample time (anywhere from a few seconds to several minutes). One of these umbilic defects, however, would attract the toron until the two rested tangentially in a similar fashion to that of an electric dipole (see Figure 6b). It was necessary to wait for the other additionally spawned defects to annihilate in order to avoid interference with the motion of the toron-umbilic pair. Once the toron and umbilic were resting adjacently in a uniform TIC, the gated signal was applied.

To measure the speed, videos at two frames per second (2 fps) were taken for 540 frames (4.5 minutes) or until the toron-umbilic pair left the frame of the video. These videos were analyzed using the video processing software ImageJ, which allowed for the tracking of the center of the toron, yielding its position in the x-y plane for each frame. The data were evaluated using the following equation: $d(x,y) = \sqrt{(x-x_0)^2 + (y-y_0)^2}$. The value *d* gives the distance of the center of the toron from its initial position (x_o, y_o) in pixels. Plotting d for each frame produced graphs such as Figure 9, and later pixels were converted to microns (6.8111 pixels = 1 micron) and frames were converted to seconds (2 frames = 1 s). By dividing the total distance traveled by the total time elapsed, a value for the average velocity was obtained. This method for calculating the speed assumed that the trajectory of the toron-umbilic pair was linear. Thus, if the motion deviated from a linear path, then an amount of the total distance traveled was lost, and thus the calculated speed was lower than the speed of the system itself.

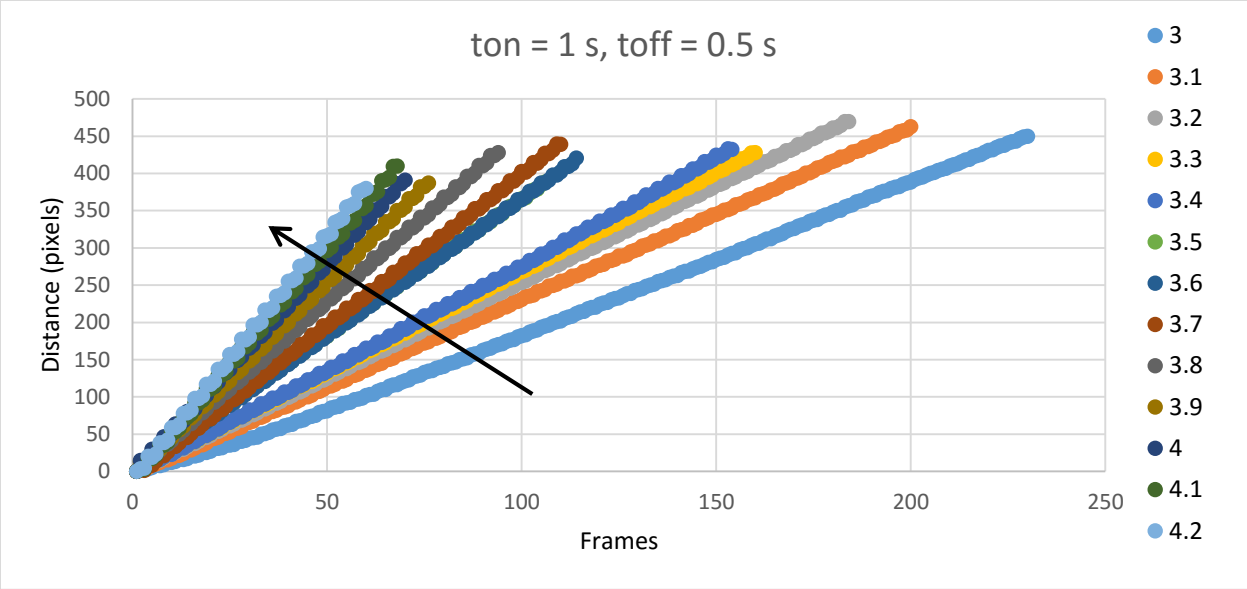

Figure 9 | An exemplary plot of the initial data obtained from a parameter sweep experiment. Each line represents the trajectory of a toron for a corresponding root-mean-square amplitude, which are indicated in the right (all measured in volts). The on and off-times were fixed at 1 s and 0.5 s respectively. Speeds were calculated by averaging the total distance traveled over the total elapsed time. The black arrow indicates the trend of the plot: higher applied voltages produced steeper slopes.

2.2.2 The Process of Attraction

In addition to the parameter sweep experiments, the details of the process of attraction of toron-umbilic pairs were investigated directly by observing a toron and umbilic as they drifted towards one another in a TIC for different applied voltages. A single toron was generated in the same cell of LC confined between polyimide-coated ITO-substrates. A root-mean-square voltage of 4 V at 1 kHz in the form of a square-wave was applied to the sample and after allowing sufficient time to pass, a toron-umbilic pair sat in equilibrium surrounded by a TIC. To observe the process of attraction, the toron and umbilic first needed to be separated. This was accomplished by trapping the toron via the optical tweezers and swiftly dragging it away from its umbilic. The field needed to be reduced to 3.6 V during this process to put the toron in a more stable state in order to avoid accidental annihilation. Once separated, the

toron was relocated approximately 200 microns away from the umbilic and then released. Upon being released, the toron and umbilic slowly drifted toward one another (see Figure 10). At this point, the voltage was changed from 3.6 V to the experimental value. Four experimental values were chosen (3.6 V, 3.8 V, 4.0 V, and 4.2 V) and three videos were recorded for each value. These values were chosen to cover the spectrum of values that were high enough to support a uniform TIC while remaining below the threshold of the toron-umbilic pair annihilation.

Video capture did not begin until the separation distance of the toron and the umbilic was approximately 75 microns (well within the frame of the CCD). The reason for the large initial separation distance of 200 μm was to allow time for the fluctuations within the TIC created by dragging the toron to settle. Videos were taken at 10 fps and lasted until the pair was at rest in equilibrium.

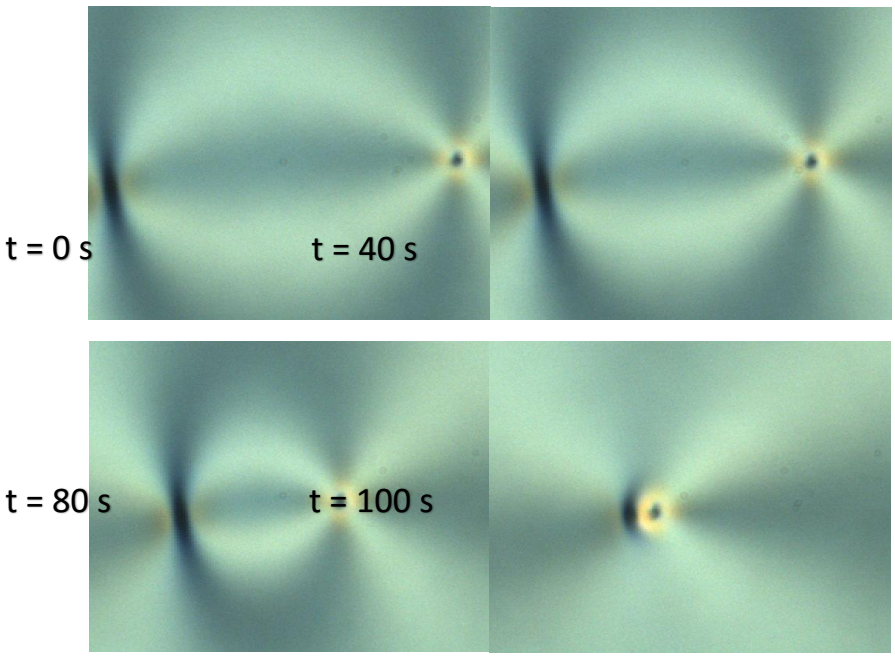

Figure 10 | A diagram of the time evolution of the process of attraction for V_{rms} = 4.2 V. The defects drift towards one another, traveling approximately 65 microns in 100 seconds.

The videos were analyzed in a similar fashion to the videos documenting the parameter sweep. However, ImageJ was used to track not only the center of the toron, but also that of the umbilic, yielding their positions in the x-y plane for each frame. The data were analyzed using the following formula: $d(x,y) = \sqrt{(x-x_0)^2 + (y-y_0)^2}$. Here, d represents the distance of each particle from the final position of the toron (x_o, y_o). This yielded data/plots shown in Figure 11. These graphs revealed 2 distinct regimes: a linear regime for large separation distances (> ~30 μm) and a nonlinear regime from smaller separation distances. The motion in the linear regime was analyzed for separation distances between 50 and 35 μm. Since the motion was linear, the speed of each defect was easily calculated by dividing 15 μm by the time taken for the defects to traverse the region of interest. The values of the defect speeds for each of the three videos corresponding to the experimental amplitude values were then averaged to provide a more accurate experimental value.

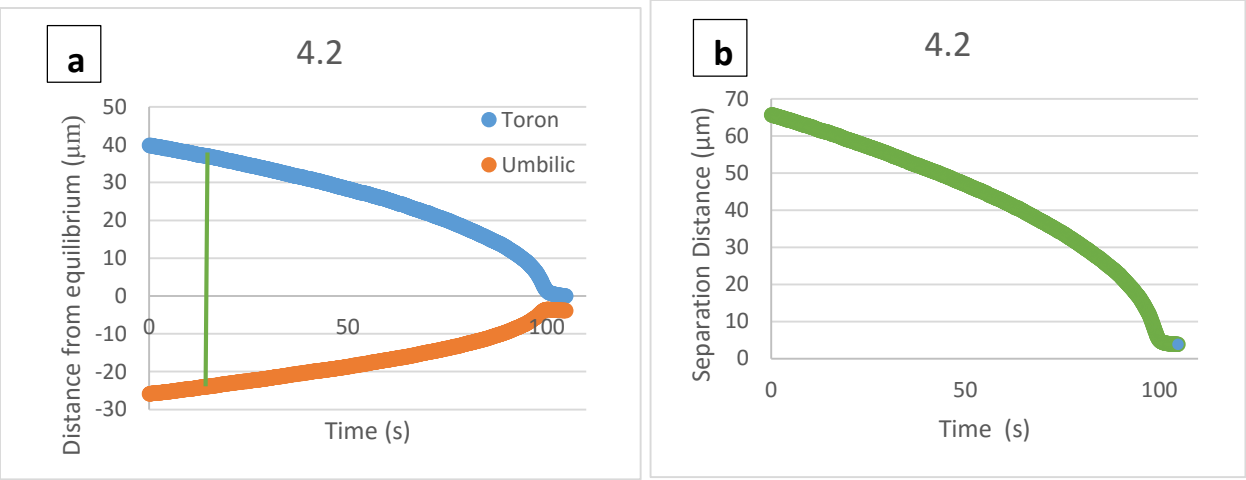

Figure 11 | Plots of the data taken from the attraction experiments. (**a**) The distance of both the toron and the umiblic from the equilibrium position of the toron as functions of time. The green line indicates the separation distance. (**b**) The separation distance as a function of time calculated from (a).

When the system underwent swimming motion, the separation distances of the toron and the umbilic remained small (< 20 μm). Thus it was of interest to discover the details of the motion for small separtion distances. This regime, however, did not exhibit linear motion, and thus could not be determined accurately by averaging the displacement divided by the elapsed time. Instead, high speed videos (150 fps) of the attraction process were recorded. Derivatives of the trajectories of each of the defects were taken, yielding values of the speeds of the defects as they approached one another. This method allowed for an accurate analysis of the motion in the non-linear regime.

2.2.3 Additional Experiments

A high speed video of a toron-umbilic pair performing two swimming-cycles under the influence of a signal with f_g = 2 Hz and dc = 50% was taken. The center of the toron was tracked, and the video provided great detail of the motion.

The effect of an additional parameter, the fill pecent (fill%), was also measured. Fill% introduces a non-zero voltage during the off-time portion of the signal and is calculated as the ratio of the magnitude of the on-time potential over the magnitude of the off-time potential (U_1/U_2). The speed of a toron-umbilic pair was measured for fill% values ranging between 30% and 100% in intervals of 10%.

To test the other manifestation of motion observed for high gate-frequencies, the speed of a toron-umbilic pair was measured as a function of gate frequency for values ranging between 1 and 100 Hz. This range extends far beyond the range covered in the parameter sweep, allowing for the system to transition from swimming motion to the drifting motion in the opposite direction. To account for the change in direction, the data were analyzed by translating the coordinates imposed on the system such that the x-axis lied along the dimension connecting the centers of the defects. The movement of the center of the toron was then tracked along this axis.

3. Results

3.1 Parameter Sweeps

3.1.1 Off-Time

The speed of a toron-umbilic pair was measured for four fixed on-times: 0.5 s, 1.0 s, 2.0 s, and 8.0 s. The off-time was varied from 0 s to 1 s in intervals of 0.1 s, however, intervals of 0.05 s were used for $0 < t_{off} < 0.5$ s for $t_{on} = 0.5$ s. The graphs of the speeds for each off-time are shown in Figure 12.

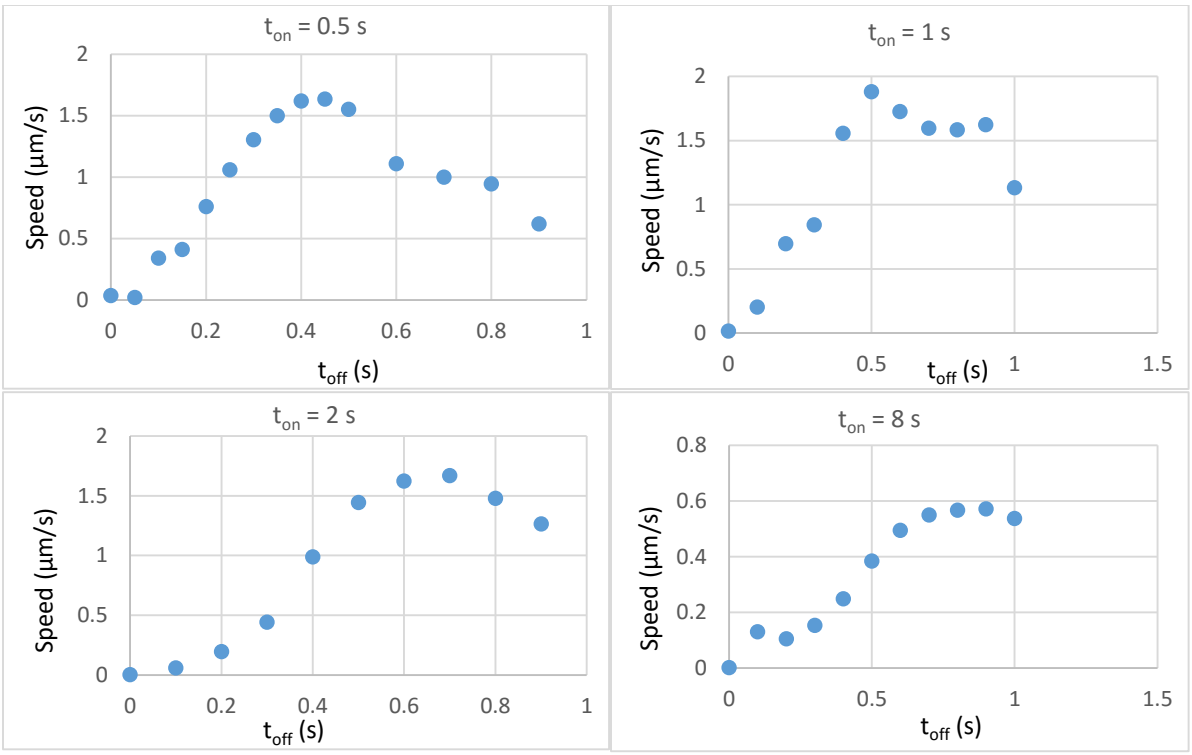

Figure 12 | Plots of the speed of a toron-umbilic pair as a function of off-time for four on-times. The gate-frequency and the duty cycle were simultaneously manipulated to achieve these value of on and off-times, while the amplitude was held constant at 4 V.

The speed increased as the off-time was increased from zero, but began to decrease after a certain threshold. Each on-time had a different corresponding off-time for which the maximum velocity was achieved. In fact, longer on-times required longer off-times to achieve this velocity. The three plots with the lowest on-time had similar maximum speeds of around 1.75 µm/s, while eight seconds of on-time resulted in much slower speeds due to low gate-frequency values.

As the electric field was turned off, the LC began to transition from a TIC to a uniformly vertically aligned director field surrounding the toron. This transition, however, did not happen instantly; instead, the LC gradually transitioned due to the absence of the electric field. When the electric field was re-applied, the LC returned to a TIC in a very short time if the off-time was

short enough. It was observed that for longer off-time, the TIC was less uniform upon the reapplication of the electric field, indicated by the presence of spontaneously formed defects and contrasting textures. Thus, if the electric field was absent for too long, a uniform TIC could not be instantly reinstated.

The cause of the decrease in the speed was exactly this; the off-time became too large and the uniformity of the TIC diminished upon reapplying the electric field, spawning new defects and external influences in the system. This caused the pair to deviate from a linear trajectory, resulting in a decreased value for the speed. As off-time proceeded even further past the maximum speed, the quality of the TIC diminished further, introducing more external influences. Once t_{off} was assigned to large enough values, the TIC would become far from uniform and the system would exhibit motion in random directions due to a large number of external influences. This can be observed in the following data set, which sweeps the gate frequency.

3.1.2 Gate Frequency

The speed of a toron-umbilic pair was measured as a function gate frequency for two duty cycles: 75% and 50%. The gate frequency values and corresponding on- and off-times used for the experiments are provided in Figure 13.

dc = 75%			dc = 50%		
f (Hz)	t on (s)	t off (s)	f (Hz)	t on (s)	t off (s)
0.25	3	1	0.25	2	2
0.3	2.5	0.8333	0.5	1	1
0.4	1.875	0.625	0.75	0.6667	0.6667
0.5	1.5	0.5	1	0.5	0.5
0.6	1.25	0.4167	1.25	0.4	0.4
0.7	1.0714	0.3572	1.5	0.3333	0.3333
0.75	1	0.3333	1.75	0.2857	0.2857
0.8	0.9375	0.3125	2	0.25	0.25
0.9	0.8333	0.2778	2.25	0.2222	0.2222
1	0.75	0.25	2.5	0.2	0.2
1.25	0.6	0.2	2.75	1818	0.1818
1.5	0.5	0.1667	3	0.1667	0.1667
1.75	0.4286	0.1428			
2	0.375	0.125			
2.25	0.3333	0.1111			
2.5	0.3	0.1			
2.75	0.2727	0.0909			
3	0.25	0.0833			
3.5	0.2143	0.7141			
4	0.1875	0.0625			
5	0.15	0.05			

Figure 13 | A table of the gate-frequency values used to measure speed for duty cycle values of 75% and 50%, along with the corresponding on and off-times.

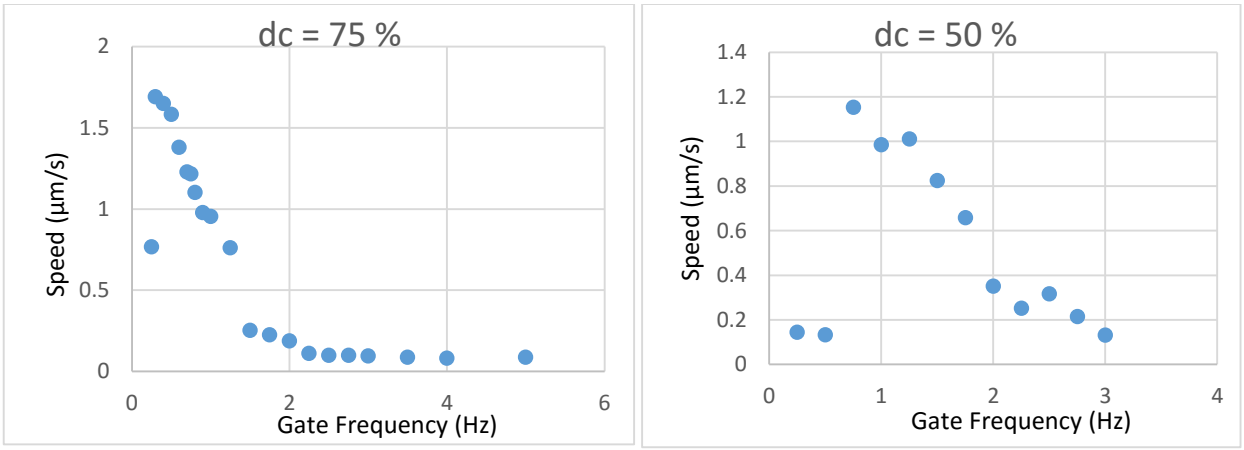

Figure 14 | Plots of speed vs. gate frequency for duty cycles of 75% and 50%. For the specific values of the gate freuncies, see Figure. The amplitude was fixed at 4.0 V.

As the gate frequency increased, the overall period of one on-off cycle decreased, resulting in shorter off- and on-times. However, since the duty cycle was fixed, the ratio of on-to-off-time remained constant. For very low values of gate frequency, long off and on-times were experienced. As discussed earlier, long off-times can cause a non-uniform TIC, inhibiting the linearity of motion and thus decreasing the calculated speed. This is shown in Figure 14, as the graphs show a sudden decrease in speed for low gate-frequency values. The drastic transition represents the threshold of relative on- and off-times for which a uniform TIC can

persist. For 50% duty cycle, an explicit cessation of linear motion is observed for low gate frequency, resulting in calculated speeds of nearly zero.

From Figure 14, it can be concluded that the maximum velocity is attained for the lowest gate frequency value for which a uniform TIC can be maintained. This is observed for both plots since the peak speeds occur immediately before the gate frequency becomes too small to maintain a uniform TIC. This indicates that less frequent, longer periods of attraction and repulsion result in faster motion. It was observed that longer on- and off-times resulted in faster motion despite performing fewer cycles over time.

Increasing the gate frequency beyond the threshold value for a uniform TIC decreased the speed, ultimatley resulting in off- and on-times too short to allow for significant separation and attraction. Inhibiting separation did not allow for the anisotropy of the velocities of the toron and umbilic to manifest, and thus no net displacement occurred.

3.1.3 Amplitude

The speed of a toron-umbilic pair was measured as a function of amplitude with the other parameters fixed at four sets of values corresponding to the values for which maximum velocity was achieved for the off-time parameter sweep (see Figure 15). The amplitude was varied from 3.4 V to 4.2 V in intervals of 0.1 V. Around 3.4 V, the electric field became too weak to create a uniform TIC. Above 4.2 V, the toron and umbilic annihilated.

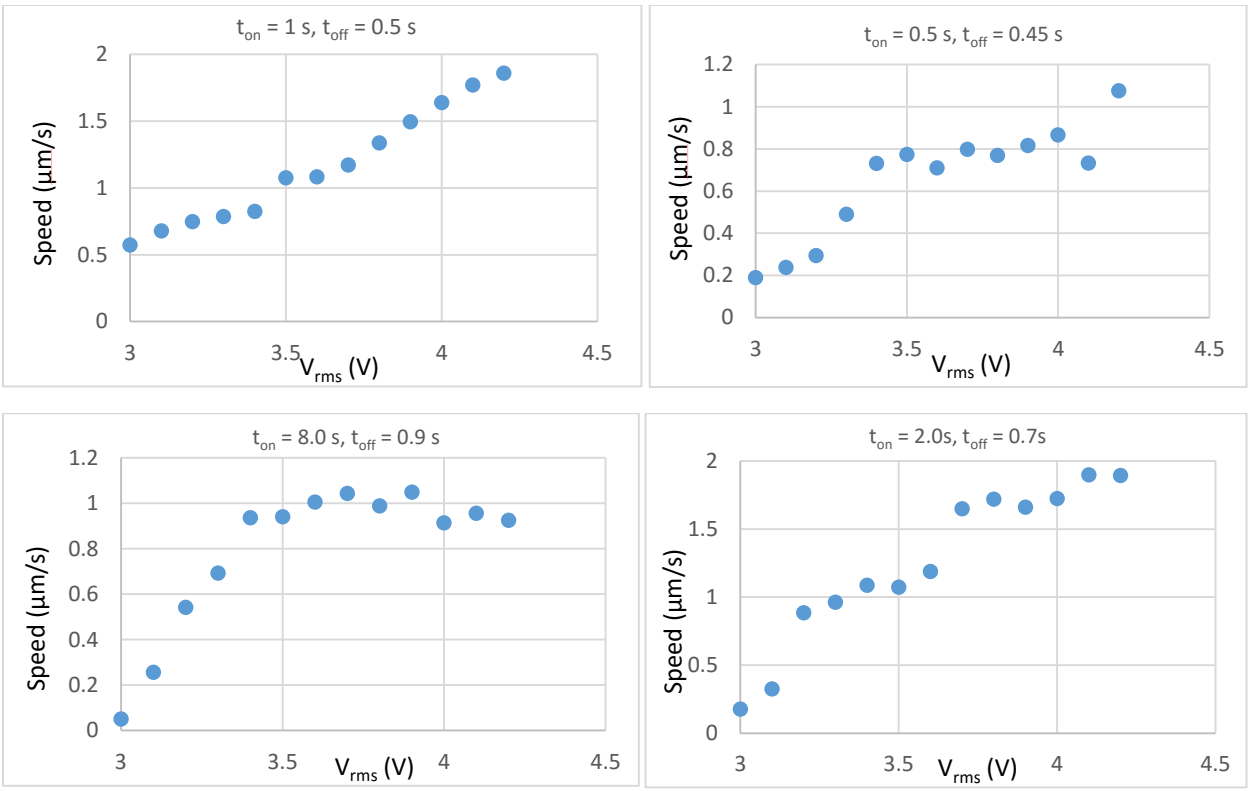

Figure 15 | Plots of speed vs. peak-to-peak amplitude of the electric field. The values of the on and off-times are provided in the titles of the graphs.

The amplitude changed the strength of alignment of the director field. Thus, greater amplitudes tend to create a higher quality TIC in shorter amounts of time due to the impetus for the director field to align in plane. For low amplitudes, slower speeds were observed (Figure 15). A uniform TIC was not observed in the sample when V_{rms} was below 3.4 - 3.5 V. For the three lowest gate frequency values, the speed increased with amplitude up to the point of annihilation. For 8 s on-time, however, the speed leveled off at around 1 µm/s when V_{rms} surpassed 3.3 V.

3.2 Process of Attraction

The speeds of the defects calculated in the linear regime of the attraction process are shown in Figure 16a. A distinct feature of graph (a) is that the toron always traveled faster than

the umbilic; this was true for each of the 12 recorded videos. Increasing the voltage proved to increase the speed of the defects for the lower amplitude values (3.6 – 3.8 V), however, the speeds did not increase above 4.0 V. Overall, the drift velocities were quite slow when compared to the speed of the swimming motion.

With the data from (a), the speed anisotropy for each applied voltage was calculated. Speed anisotropy is defined as the difference of the speed of the defects; simply the speed of the umbilic subtracted from the speed of the toron. While graph (b) shows a slight increase in the speed anisotropy with respect to applied voltage, there was very little variance in the values; the applied voltage had little effect on the speed anisotropy. Since the defect speeds increased between 3.6 and 4.0 V but the speed anisotropy remained nearly constant, it can be concluded that increasing the voltage affects both the speeds of the toron and the umbilic in equal amounts.

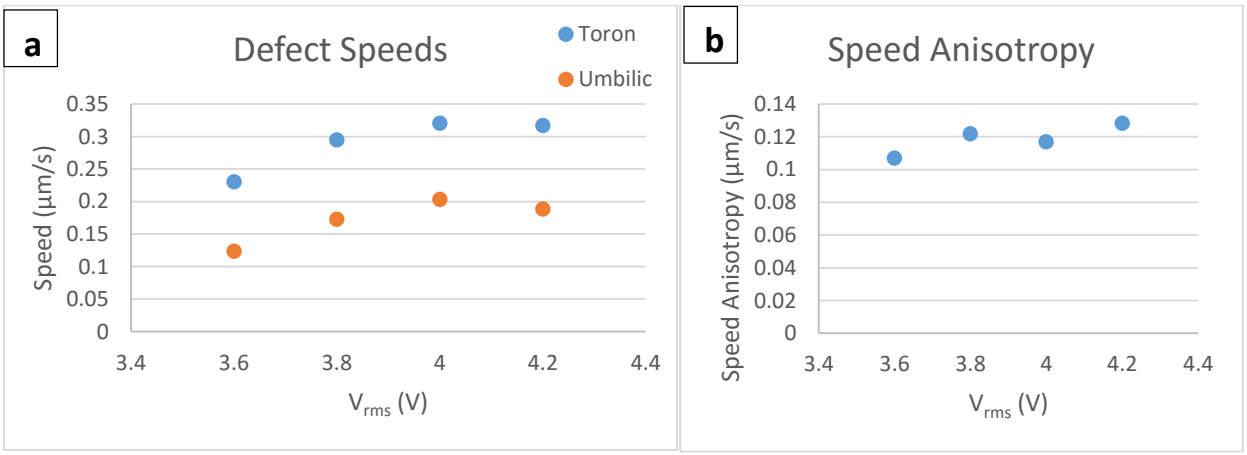

Figure 16 | (**a**) The average speed of both the toron and the umbilic during the process of attraction for four different applied voltages. Each data point is an average of three measurements. (**b**) The speed anisotropy of the average defect speeds.

To analyze the motion of the defects in the non-linear regime, time derivatives of the trajectories of both the toron and the umbilic during the process of attraction for two different different applied voltages were taken (see Figure 17). The derivatives provided values of the speed at each moment in time. Note that the velocities of the umbilics are positive due to the arbitrary choice of coordinates; the signs of the velocities represent the relative difference in the directions of motion, however, the signs themselves are irrelevant.

An anisotropy was observed in the speed of the defects with the toron moving faster than the umbilic. This anisotropy increased dramatically around 30 seconds as the toron experienced a large increase in speed. Over a period of about 2.5 s, the speed of the toron changed by 70 μm/min while the umbilic experienced a change of 15 μm/min. In other words, as the toron and umbilic approached small separation distances, the toron jolted towards the umbilic. The umbilic also experienced an increase in speed, however the toron's peak speed was more than two times that of the umbilic. This large speed anisotropy explains the net displacement observed during the swimming process. In close proximity, the toron rapidly accelerates towards the umbilic, causing the system to come to an equilibrium state some distance in the direction of the umbilic from its initial position.

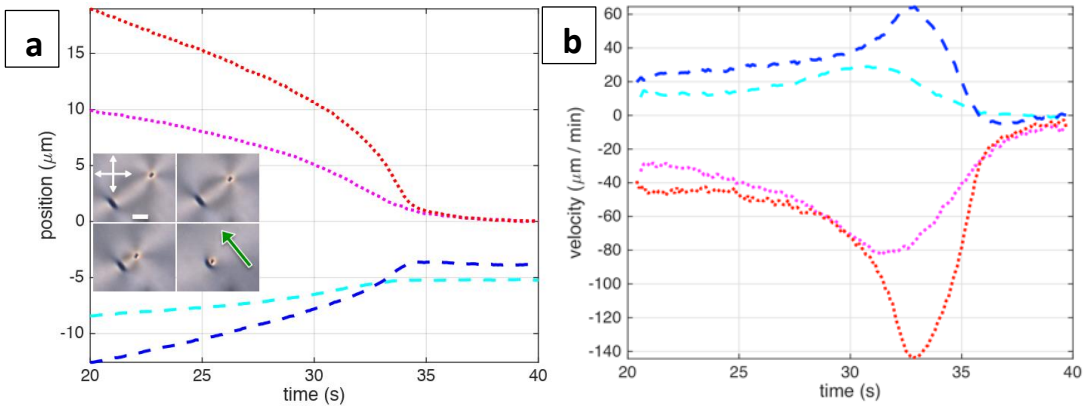

Figure 17 | (**a**) Toron (dotted lines) and umbilic (dashed lines) distances from the final resting position of the toron center plotted vs. time for 4 V_{rms} (red and blue) and 3.75 V_{rms} (magenta and cyan). The inset images show images from the movie used to track the toron and umbilic for 4 V_{rms}. The double-headed white arrows denote transmission axis of polarizers and the green arrow denotes the c-field orientation. (**b**) Velocity analysis of the same video used in (a).

3.3 Additional Experiments

Figure 18a shows the trajectory of the center of a toron during two swimming-cycles. With a toron-umbilic pair initally in equilibrium, a signal with a gate frequency of 2 Hz and a duty cyle of 50% was applied. Upon the cessation of the electric field, the toron moved quickly in the direction opposite that of the umbilic. Once the field was reinstated, the toron drifted towards the umbilic's new location. During this process, the toron traveled beyond its initial location, leaving the system displaced in the direction of the umbilic. As the field turned off for the second time, the toron again moved away from its umbilic and the cycle repeated. This caused the toron to again surpass its previous position, leaving the system futher displaced in the direction of the umbilic. As the field remained constant, the toron-umbilic pair drifted slightly.

The effect of fill% on the speed of a toron-umbilic pair undergoing swimming motion is shown in Figure 18b. It was expected that the speed would decrease to zero as U_1/U_2

approached 1 since the signal would be in a constant on-state leaving the toron-umbilic pair in equilibrium. The motion, however, changed its direction for fill% values within the range of 60 – 90%. When fill% was large, a TIC was maintained and the toron-umbilic pair was unable to achieve a significant separation distance. Instead, the system exhibited very slow vibrational motion in the direction of the toron, or the direction opposite that of swimming.

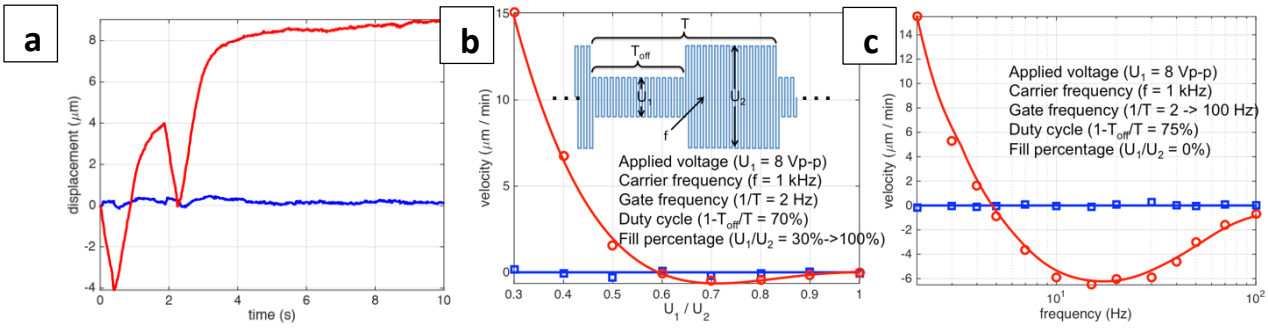

Figure 18 | (**a**) The trajectory of two swimming-cycles with the toron-umbilic pair initially in equilibrium. The red line represents the motion of the toron in the direction of the umiblic and the blue line represents motion along the perpendicular direction. (**b**) Velocity of a toron-umbilic pair plotted as a function of U_1/U_2 perpendicular to the c-field (red circles) and parallel to the c-field (blue squares). Inset shows experimental parameters of the amplitude modulated square wave signal used in experiments. (**c**) Velocity of the toron-umbilic dipole plotted as a function of gate frequency (ranging from 2 to 100 Hz), U_1 = 4 V_{rms}, U_2 = 0 V_{rms}, and dc = 75%, perpendicular to the c-field (red circles) and parallel to the c-field (blue squares).

A similar phenomenon was observed for the motion resulting for high gate frequency values (see Figure b). Above 5 Hz, the toron-umbilic pair began exhibiting vibrational motion in the direction of the toron. The speed continued to increase, reaching a peak of 6 μm/min for a gate frequency value of about 20 Hz. Upon further increasing the frequency, the speed gradually diminished, reaching a value near zero at 100 Hz. This motion can also be credited to the lack of separation distance achieved by the toron-umbilic pair.

4. Discussion

4.1 Defect Dynamics

From the results of both the gate-frequency and the off-time parameter sweeps, it can be concluded that maximum speed is achieved for the smallest gate frequency above the threshold for maintaining uniform TIC and that longer on-times require longer off-times to achieve maximum speed. Therefore, it can be deduced that longer on-time allows for longer off-times without resulting in a loss of TIC uniformity. In other words, the ability of the LC to reconfigure into a uniform TIC upon the reapplication of the electric field increases with on-time.

Amplitude was found to increase the speed of the swimming motion of toron-umbilic pairs. The speeds of the individual defects during the process of attraction were also shown to increase for low applied voltage, but were affected less at higher voltages. Related work was done on the effect of applied voltage on the drift velocity of +1 and -1 umbilic defects. Dierking et al. observed two oppositely charged defects as they approached each other to annihilate and measured the velocities of each defect along with the speed anisotropy (see Figure 19a)[2]. As the amplitude of the applied AC electric field was increased, the speed of the defects decreased. This was also attributed to the effect of overlap, since decreasing the magnitude of the electric field results in greater overlap of energetically costly distortions. The speed anisotropy was unaffected (see Figure 19b)[2].

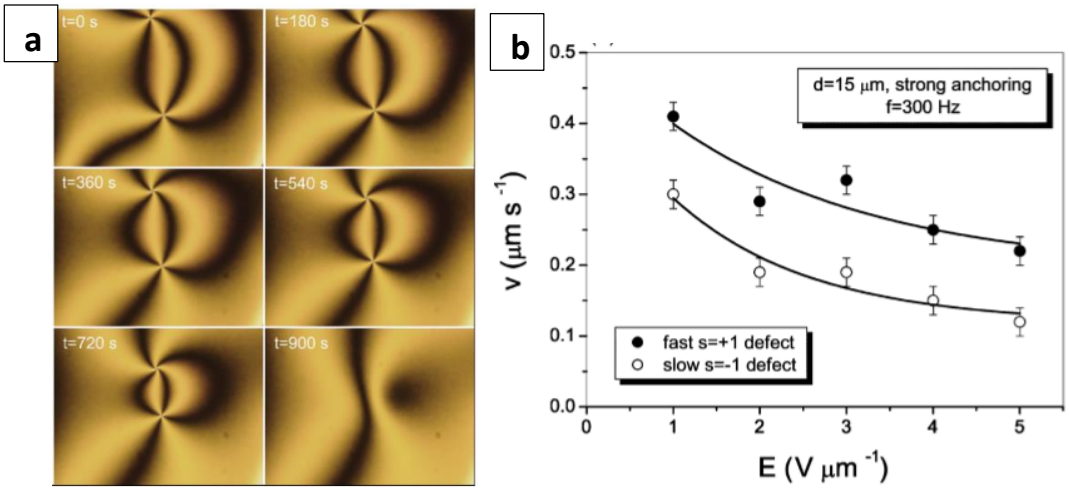

Figure 19 | Images taken from [2]. (**a**) Exemplary texture series illustrating the time evolution of a pair of umbilical defects during the defect annihilation process. The applied field is 1 V μm^{-1}, frequency f = 300 Hz, and cell gap d = 50 μm. Each image shown in approximately 350 x 500 micrometers^2. (**b**) Defect speeds of the fast and slow defect during the annihilation process as a function of applied electric field amplitude for a cell with strong homeotropic anchoring conditions^2.

The effect of applied voltage on the speed of the toron and umbilic system follows a trend opposite that of the umbilic defects studied by Dierking et al.; the speed of the toron and the umbilic tended to increase while the +1 and -1 defects tended to decrease with respect to increasing applied voltage. Therefore, the effect of backflow cannot be the only factor affecting the toron-umbilic system. The speed anisotropy, however, of both systems remained relatively constant.

The ideas drawn from the experiments of Dierking et al., however, can still be applied to systems of torons. Backflow of LC into the region behind the moving defects was attributed to the speed anisotropy of the umbilic defects^2. This could potentially explain the speed anisotropy of the toron and its umbilic. Also, their speeds were attributed to the amount of overlap between the distortions associated with the defects. With a greater electric field, there was less overlap and the speeds of the defects decreased. Since the size of the torons decreases with respect to applied voltage, overlap of the toron and the umbilic is greater for

lower voltages. This phenomenon, however, cannot be the sole contributing factor to the motion of the defects since their speeds increased with applied voltage. Therefore, another factor must be present to cause the speed of both the toron and the umbilic to increase for low applied voltages.

Since the defects studied in the Dierking et al. experiments differed greatly from the toron-umbilic systems, it is likely that the cause for the different trends can be attributed to the difference in topological structure. The locality of the umbilical defect associated with the toron is greatly affected by applied voltage; it's size increases greatly with decreasing voltage, especially when it is separated from its toron. For very low voltages (< 3.4 V) the umbilic can actually extend and become a wall defect within the TIC. The locality of the umbilic may have a large effect on its attractive force with the toron causing the speed of the defects to decrease at lower voltages. The slight decrease in speeds from 4.0 V to 4.2 V may be attributable to the effect of backflow becoming dominant.

In the non-linear regime, the speeds of the defects increased rapidly. The speed anisotropy also increased as the toron moved rapidly towards the umbilic. This mechanism is responsible for the swimming motion observed by toron-umbilic pairs; as the two defects drift towards one another, the toron travels much faster than the umbilic, resulting in a net displacement of the system.

The alternative form of motion exhibited by toron-umbilic pairs occurred for fill%'s within the range of 60% and 90% and also for gate frequencies within the range of 5 and 100 Hz. This motion was caused by the inability of the system to achieve large separation distances

and propelled by the repulsion of the toron corresponding to the electric-field signal turning off.

4.2 CF-2 Drift

Research has also been done on the dynamics of related cholesteric structures in LC, known as cholesteric fingers of the second type (CF-2s). CF-2s manifest due to the twisting nature of chiral nematic liquid crystals (CNLCs) and the director rotates 2π radians across the mid-plane of the CF-2.

Baudry et al. tested the drift velocity of CF-2s in an AC electric field as a function of the conductivity of the LC. They observed fingers drifting perpendicularly to their axes[4]. The drift velocities of CF-2s were measured for different electric conductivities as a function of the amplitude and frequency of the AC electric field. It was found that for low frequencies, the conductivity had no effect on the drift velocity, while for high frequencies, the velocity strongly decreased. The amplitude was shown to increase the drift velocity[4]. The pre-existing model for CF-2 drift, the Gil and Gilli model, could not explain the dependence on conductivity[2]. The authors suggested that a Carr-Helfrich effect be considered.

Tarasov et al. were able to explain the motion of CF-2s by means of the Carr-Helfrich effect. They attributed the driving mechanism for chirality-related dynamic phenomena to electro-hydrodynamic effects, under which the Carr-Helfrich effect is classified[3]. The proposition was that flow and differences in pressure, which can be produced by moving charges within the sample, are the driving mechanism behind the motion of the defects.

Despite the similarities of the systems, the Carr-Helfrich effect cannot be attributed to the motion of toron-umbilic pairs in gated electric fields. The reason for this is that electro-hydrodynamic effects are suppressed for electric fields of the order of 1 kHz since the charges are not given sufficient time to travel but instead are being pulled back and forth extremely quickly. It is interesting to note that our system is chiral, which could be important in explaining the observed motion in the absence of Carr-Helfrich.

4.3 Applications

Topological defects are an important topic of study in discovering the physics of the early universe. The relativity and gravitation group at the University of Cambridge stated, "Their [topological defects] study is an unavoidable part of any serious attempt to understand the early universe."[13]. Phase transitions occurred during the time of the early universe, which caused defects to appear. These cosmological defects have not yet been detected and are nearly impossible to reproduce. Defects within liquid crystal, therefore, provide a means of studying topological defects to aid in the understanding of their role in the evolution of the universe. More generally, nematic liquid crystals are model experimental systems for the physics of topological defects[15].

The dynamic properties of toron-umbilic pairs also aids in the understanding of active-matter systems. Active matter is defined as "An assembly of self-driven units that take energy from the environment to produce motion"[14]. Examples of such systems are mammal herds, bird flocks, cell tissue and self-propelled colloids. These systems, however, are not simple to study. Thermodynamic quantities are often hard to define in active systems since the transfer

and dissipation of energy into the system occurs by different mechanisms than those of non-active systems[14]. Therefore, a complete statistical framework is missing within the description of active matter. Since the development of statistical mechanics was driven by the kinetic theory of gases, it has been postulated that a description of active matter will evolve first with kinetic theories of interacting self-propelled particles[14].

5. Conclusion

In conclusion, toron-umbilic pairs exhibited a distinctive swimming-like motion when exposed to a gated electric field. The speed of the ensembles increased with the magnitude of the applied field and was maximized for the the longest off-time while still maintaining a uniform TIC. A speed anisotropy was observed in the speeds of the toron and the umbilic and was determined to be the mechanism behind the resulting net-displacement of the system.

Another manifestation of motion was observed and occurred in the direction opposite that of the swimming motion. By inhibiting the ability of the toron-umbilic pair to separate, the instant repulsion of the toron propelled the system. To accomplish this, either the fill% or the gate frequency had to be increased to sufficiently high values effectively reducing the toron-umbilic separation during one modulation cycle. This probes a different regiem of the toron-umbilic interaction and enable directional control of the defect ensemble motion.

These forms of motion cannot be attributed to the theories underlying the dynamic properties of CF-2s and umbilic defects alone (Carr-Helfrick and backflow repsectively). Instead, the toron-umbilic system exhibits unique dynamic properties of defect ensembles due to the

combination of elastic interactions, backflow and various timescales associated with the LC viscosity.

While this research serves as a first-step analysis of the system, additional work can be done. Finding means to effectively track the umbilic during the separation process would aid in the understanding of the speed anisotropy of the defects, and thus the mechanism behind swimming motion. Numerical modeling the effect of elastic anisotropy, backflow, and viscosity anisotropy in this system would also provide additional details of the speed anisotropy. The effect of cell width on the motion of toron-umbilic pairs could also be determined. Finally, testing this phenomenon in non-chiral systems may help attribute the dynamic properties to the cholesteric nature of the LC.

6. References

1. Ackerman, P. J., van de Lagemaat, J. & Smalyukh, I. I. Self-assembly and electrostriction of array and chains of hopfion particles in chiral liquid crystals. *Nat. Commun.* **6**, 6012 (2015)
2. Dierking, I. *et al.* Anisotropy in the annihilation dynamics of umbilic defects in nematic liquid crystals. *Phys. Rev. E* **85**, 021703 (2012)
3. Tarasov, O. S., Krekhov, A. P. & Kramer, L. Dynamics of cholesteric structures in an electric field. *Phys. Rev. E* **68**, 031708 (2003)
4. Baudry, J., Pirkl, S. & Oswald, P. Effect of the electric conductivity on the drift velocity of the cholesteric fingers of the second type in confined geometry. *Phys. Rev. E* **60**, 2990 (1999)
5. Baudry, J., Pirkl, S. & Oswald, P. Looped finger transformation in frustrated cholesteric liquid crystals. *Phys. Rev. E* **59**, 5562 (1999)
6. Senyuk, B. Liquid Crystals: A Simple View on a Complex Matter. < http://www.personal.kent.edu/~bisenyuk/liquidcrystals/intro.html>
7. Andrienko, D. Introduction to liquid crystals. < http://www2.mpip-mainz.mpg.de/~andrienk/teaching/IMPRS/liquid_crystals.pdf> (2006)
8. Fukuda, J., Zumer, S. Quasi-to-dimensional Skyrmion lattices in a chiral nematic liquid crystal. *Nat. Commun.* **2**, 246 (2011)
9. Murphy, A. Blue Phases in Liquid Crystals < http://guava.physics.uiuc.edu/~nigel/courses/569/Essays_Fall2011/Files/murphy.pdf>
10. Fernsler, J. Liquid Crystals < http://www.calpoly.edu/~jfernsle/Research/Liquid%20Crystals/LCResearch.html>
11. Sethna, J. P. Order parameters, broken symmetry, and topology < http://www.lassp.cornell.edu/sethna/OrderParameters/TopologicalDefects.html>
12. Smith, S. P. *et al.* Inexpensive optical tweezers for undergraduate laboratories. *Am. J. Phys.* **67**, 1 (1999)
13. <http://www.damtp.cam.ac.uk/research/gr/public/cs_top.html>
14. Bertin, E. An equation of state for active matter. *Am. Phys. Soc. Physics* **8**, 44 (2015)
15. Araki, T., Serra, F., Tanaka, H. Defect science and engineering of liquid crystals under geometrical frustsration. *Soft Matter*, **9**, 1807 (2013)
16. Kléman, M. Defects in liquid crystals. *Reports on Progress in Physics*, **52(5)**, 555. (1989)